

We are IntechOpen, the world's leading publisher of Open Access books Built by scientists, for scientists

6,900

Open access books available

186,000

International authors and editors

200M

Downloads

Our authors are among the

154

Countries delivered to

TOP 1%

most cited scientists

12.2%

Contributors from top 500 universities



WEB OF SCIENCE™

Selection of our books indexed in the Book Citation Index
in Web of Science™ Core Collection (BKCI)

Interested in publishing with us?
Contact book.department@intechopen.com

Numbers displayed above are based on latest data collected.
For more information visit www.intechopen.com



Structure of Clays and Polymer–Clay Composites Studied by X-ray Absorption Spectroscopies

Gustavo M. Do Nascimento

Additional information is available at the end of the chapter

<http://dx.doi.org/10.5772/61788>

Abstract

A wide range of spectroscopic techniques employ higher-energy electromagnetic radiation, ranging from vacuum UV ($\approx 10\text{--}40$ eV, 125–31 nm), including soft X-rays (40–1500 eV, 31–0.8 nm), and going to hard X-rays ($1500\text{--}10^5$ eV, 0.8–0.01 nm) for elucidating molecular structures of chemical and biological interest. A typical X-ray absorption (XAS) spectrum has a large absorption near the edge followed by serial oscillations that gradually fade away. This set of oscillations extends over a wide energy range and can be divided into two regions: the absorption near the edge is called XANES (X-ray absorption near-edge structure) and the second region is the so-called EXAFS (extended X-ray absorption fine structure). The XAS data enables the determination of crystallographic parameters and also the signal intensity contains information of the oxidation state and the chemical bond in the solid. For instance, theoretical calculations were essential to verify the differences between the oxygen and silicon sites in clays. Experimental and theoretical EXAFS studies of clays with Cu(II) show that Cu(II) has interchangeable octahedral, tetragonal, and square planar coordinations in the clay interlayer, depending on Cu(II) loading and degree of hydration. XANES data of intercalated poly(aniline) show new bands at 398.8 eV and 405–406 eV, which were assigned to new chromophoric segments formed within the galleries of the Montmorillonite clay. Hence, in this chapter, this amazing new area will be reviewed concerning the state-of-the-art results of characterization of their structural features. Previous and new results of the X-ray absorption spectroscopy of clays and polymer–clay materials obtained by our group will be considered. The main goal of this work is to contribute to the rationalization of some important results obtained in the open area of clays and clay materials characterization.

Keywords: XANES, Clays, Ceramics, EXAFS

1. Introduction

1.1. Clays, clay minerals, and ceramics

The term clay can assume different meanings for different groups of people. For the farmer, clays are the mechanical and chemical environment where most plants grow. For the ceramist, it is the raw material of his works for over 4000 years. To the editor, it gives softness to the paper's surface in high-quality prints. In the medical area, it may be for the relief of diarrhea and so on. In fact, there is no uniform nomenclature for clay and clay materials [1, 2]. Georgius Agricola (1494–1555), the founder of geology, was apparently the first to propose a definition for clay [3]. The last definition is that the term clay can be considered as natural fine-grained minerals with plastic behavior at appropriate water contents that will harden when dried or fired. Generally, in the area of geology, clays are considered as particles with a size dimension of $<4 \mu\text{m}$, while in colloid science, a value of $<1 \mu\text{m}$ is more acceptable [4, 5]. Likewise, the term "clay mineral" is difficult to define. As a first approximation, the term signifies a class of hydrate phyllosilicates making up the fine-grained fraction of rocks, sediments, and soils. The definition that the JNCs have proposed is "...phyllosilicate minerals and minerals which impart plasticity to clay and which harden upon drying or firing" [3]. Since the origin of the mineral is not part of the definition, clay mineral (unlike clay) may be synthetic.

Hence, clay minerals are extremely fine materials that can only be studied in detail by using X-ray techniques or sophisticated microscopic techniques, such as the electron scanning microscope [6]. They are primarily hydrated aluminosilicates in which the magnesium and iron can replace the aluminum wholly or partly with alkaline or alkaline earth elements. Thus, its chemical composition is variable, such as the nature of the interlayer cations and water content. The different clay minerals have different dehydration properties, structural failure limits, decomposition products, cation exchange capacity (CEC), and other useful properties of economic interest.

Clays layers are formed from tetrahedral sheets in which a silicon atom is surrounded by four oxygen atoms and octahedral sheets in which a metal such as aluminum or magnesium is surrounded by eight oxygen atoms [1-3, 7]. The tetrahedral (T) and octahedral (O) sheets are bonded by the oxygen atoms. Unshared oxygen atoms are present in hydroxyl form. Two main arrangements of T and O layers are observed in major parts of clays. One tetrahedral fused to one octahedral (1:1) is known as the kaolin group, with a general composition of $\text{Al}_2\text{Si}_2\text{O}_5(\text{OH})_5$ and a layer thickness of $\sim 0.7 \text{ nm}$. Phyllosilicates are formed by one octahedral sheet bonded between two tetrahedral sheets (2:1) with a total thickness of 0.94 nm . When the aluminum cations in the octahedral layers are partially substituted by divalent magnesium or iron cations, the smectite clay group is formed, whose structure consists of a central sheet containing groups $\text{MO}_4(\text{OH})_2$ of octahedral symmetry associated with two tetrahedral sheets (MO_4) producing layers designated as T:O:T (see Figure 1.) [7]. The octahedral sites are occupied by ions of aluminum, iron and magnesium, while the centers accommodate tetrahedrons of silicon and aluminum ions. The negative charges from the T:O:T lamellae are neutralized by hydrated alkaline cations that can be exchanged with any other cationic species. Mainly, smectite clays exhibit surface adsorption and catalytic activity in organic reactions.

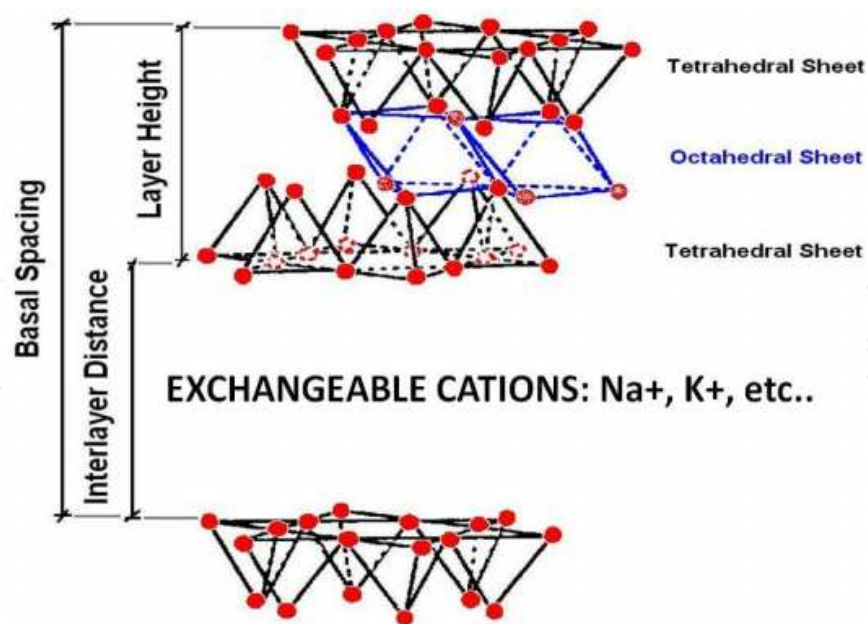


Figure 1. Schematic representation of montmorillonite clay (MMT)

Finally, the ceramics are defined [8-10] as the art and science of making products and articles (a) chiefly or entirely from "earthy" raw materials, that is, from the so-called nonmetallics excepting fuels and ores of metals; and (b) with a high-temperature treatment involved, either in manufacturing or in service. The technology of clays in the field of ceramics includes consideration of both the room-temperature properties and the behavior at elevated temperatures. When clays are used in ceramics, one of several functions is generally served. Most clays, alone or in mixtures, are used for their contribution to the working properties, drying strength of the ceramic masses which they comprise or to which they have been added. Some clays, however, are used more because they offer an inexpensive body constituent or filler of the desired chemical composition, already subdivided by nature to a convenient grain size.

1.2. Polymer–clay materials

A polymer–clay material is made by the combination of a polymer and synthetic or natural clay. The presence of clay can improve the mechanical, thermal, barrier and fire retardancy properties of the polymer. If the polymer–clay material has at least one phase with organization in the nanometer scale, the material is called a nanocomposite. It is important to emphasize that the main characteristics of the polymer–clay materials are strongly related to the physical and chemical peculiarities of each component and also due to the nano size aspect and interfacial adhesion between the nanocomposite parts [11, 12].

Polymer nanocomposites are formed at least with one part in the nanometer scale (<100 nm). Despite the term nanocomposite being very recent, in fact, has been possible to reconize in the nature a diverse range of materials, such as bones, shells and wood that can be considered nanocomposites because they are formed by carbohydrates, lipids and proteins organized in the nanometer regime [13]. In recent years, the characterization and control of structures at the

nanoscale level have been studied, investigated and exploited. Consequently, the nanocomposite technology has emerged as an efficient and powerful strategy to upgrade the structural and functional properties of synthetic polymers. Polymer nanocomposites have attracted great attention due to the exhibition of superior properties such as strength, toughness and fire barrier far from those of conventional microcomposites and comparable with those of metals. The presence of one nanoscale phase leads to tremendous interfacial contacts between the polymer and clay and, as a consequence, the improvement of the polymer bulk phase, such as mechanical, thermal, barrier, durability, chemical stability, flame retardancy, scratch/wear resistance, biodegradability as well as optical, magnetic and electrical properties [14-17]. The increased performance of the mechanical properties of nanocomposites is related to the clay content and the aspect ratio of the clay [18].

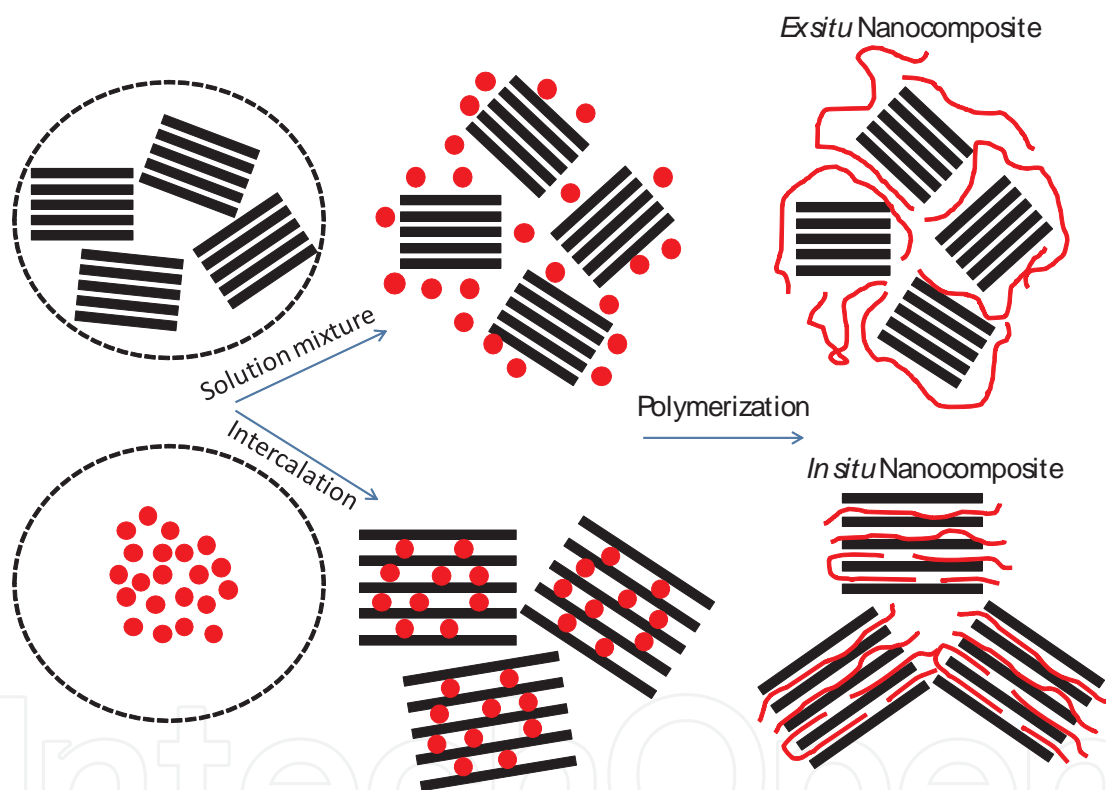


Figure 2. Schematic representation of two types of preparations of polymer-clay nanocomposites

Clays have been widely used for the preparation of polymer nanocomposites. Recently, there has been a growing interest for the development of polymer-clay nanocomposites due to their dramatically improved properties compared to conventional polymer composites in a very low fraction [19, 20]. Polymer-clay nanocomposites can be prepared by direct mixture of two aqueous solutions containing the monomer and the clay suspension (see Figure 2.); afterward, the polymer can be formed by adding a polymerization agent, or induced by thermal or light exposition. The resulting material is called an *ex situ* nanocomposite because the major part of the polymer is found outside the interspaces of the clay. It is important to mention that the initial clay concentration can be modulated and, in some cases, the clay layers are completely

separated, as a consequence, the resulting material is known as exfoliated polymer–clay nanocomposite. In a second method (see Figure 2.), the monomer is intercalated in the interlayer space of the clays by charge exchange or by diffusion inside the clay galleries previously modified with an organic salt. Afterward, the intercalated polymer can be polymerized and the resulting material is known as an *in situ* nanocomposite because the major part of the polymeric content is inside the clay interspaces.

1.2.1. Nonconducting polymer–clay materials

In this chapter, we will only provide a summary of the main characteristics found in the polymer–clay nanocomposites. Here, we divide the section between polymer–clay nanocomposites formed by intrinsic nonconducting polymers or by conducting polymers. Traditionally, the clay layers must be previously treated with an organic agent (this point was not explicitly discussed in Figure 2.) to ensure good dispersion of clay layers within the polymer matrix. The dispersion of clay plates into the polymeric matrix is very difficult, mainly by stacking forces between the clay layers and its hydrophilic character. Hence, it is necessary to modify the clay layers in order to increase the chemical compatibility with hydrophobic polymer chains. Only a few hydrophilic polymers such as polyethylene oxide and polyvinyl alcohol can be miscible with clay layers [21].

The origin of polymer–clay hybrids starts with the creation of nylon-6-clay hybrid (NCH) developed in 1986 under Toyota Central Research and Development Laboratories. Afterward, the use of modified clays as precursors to nanocomposite formation was extended into various polymer systems including epoxies, polyurethanes, polyimides, nitrile rubber, polyesters, polypropylene, polystyrene and polysiloxanes, among others. For true nanocomposites, the clay nanolayers must be uniformly dispersed and exfoliated in the polymer matrix. The presence of aggregated tactoids in conventional polymer–clay composites improves rigidity but sacrifices strength, elongation and toughness. However, exfoliated clay nanocomposites, such as NCH, show enhancement in all aspects of their mechanical performance.

1.2.2. Conducting polymer–clay materials

The intrinsically conducting polymers (ICPs), or simply synthetic metals, form one of the largest classes of molecular conductors [22]. The preparation of stable poly(acetylene) (PA) films was achieved in the 1970s by Shirakawa and Ikeda [23, 24]. However, it was only in 1977 that the possibility of doping PA using Lewis's acid (or base) was discovered [25]. During the process of doping [26, 27], the conductivity typically ranges from 10^{-10} to 10^{-5} S cm⁻¹, and the polymer is converted into a "metallic" regime. The addition of nonstoichiometric chemical species in quantities that are commonly low ($\leq 10\%$) results in dramatic changes in the electronic, electrical, magnetic, optical and structural properties of the polymer. The doping is reversible, and the polymer can return to its original state without major changes in its structure. In the doped state, the presence of counterions stabilizes the doped state. All conductive polymers, for example, poly(para-phenylene) (a), poly(*p*-phenylene-vinylene) (b), poly(pyrrole) (c), poly(thiophene) (d), poly(furan) (e), poly(heteroaromatic vinylene) (f), (where Y = NH, NR, S, O), poly(aniline) (g), poly(para-phenylenediamine) (h), poly(benzidine)

(i), poly(ortho-phenylenediamine) (j), among others (see Figure 3.), may be doped by p (oxidation) or n (reduction) through chemical and/or electrochemical process.

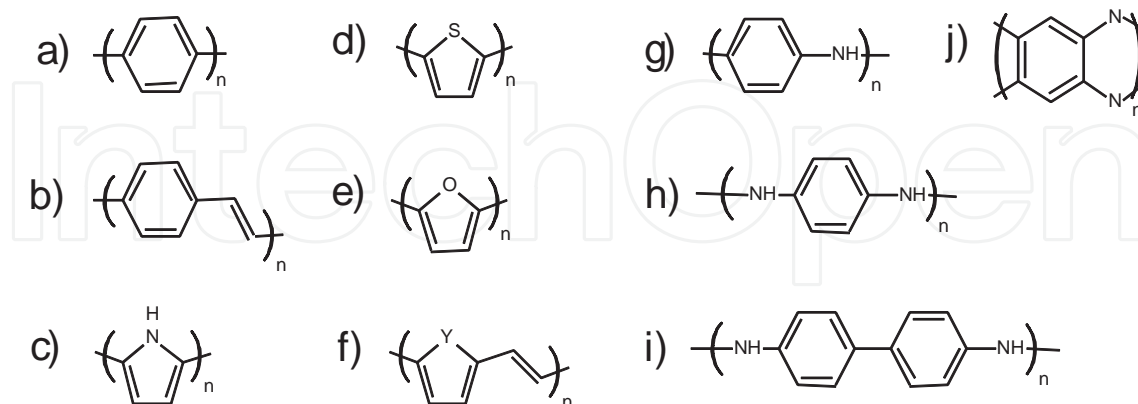


Figure 3. Schematic representation of the chemical structures of the most common conducting polymers

In this chapter, we will give special attention to the polymer–clay nanocomposites formed by polyaniline (PANI) and its derivatives. Among the different types of hosts used in the formation of nanocomposites with PANI, lamellar materials are undoubtedly the most widely employed. The main reason is that the distance between the layers can be modified, facilitating the intercalation of various chemical species. Hosts, such as MoO_3 [28], V_2O_5 [29, 30], $\alpha\text{-Zr}(\text{HPO}_4)_2\cdot\text{H}_2\text{O}$ [31], $\text{H}_2\text{UO}_2\text{PO}_4\cdot 4\text{H}_2\text{O}$ [32], FeOCl [33], layered double hydroxide (LDH) [34] and MoS_2 [35], and most frequently, clays were used for intercalation of PANI [36-50].

The adsorption of aniline on MMT clay has been studied a long time ago, and since then, it has been well-known that clays have a property to generate colored species by the adsorption of aromatic amines. The best known case is the blue color generated by the adsorption of benzidine (4, 4'-diaminobiphenyl) in clay [37]. Among the earlier studies [38-40], it was reported that films of MMT containing metal ions become black after immersion in aniline; the authors suggest that this is due to the polymerization of monomers. Soma and Soma [41, 42] and Soma et al. [43-45] used resonance Raman spectroscopy (RR) in the study of oxidation of aromatic compounds (benzene and derivatives) adsorbed on clay, and showed that when the adsorption of aniline on Cu^{2+} or Fe^{3+} -MMT is made in the liquid phase, polymer formation occurs. Soma and Soma proposed that the polymer formed was equal to that generated electrochemically (PANI-ES), but with the presence of azo linkages ($-\text{N}=\text{N}-$). Also, Mehrotra and Giannelis [46] synthesized PANI intercalated in a synthetic hectorite containing Cu^{2+} ions, the UV-vis-NIR spectrum was very similar to that observed for PANI-EB, and the polymer was converted to conductive PANI-ES form, simply by exposing the material to HCl vapors. Other work done by Chang et al. [47] reported the polymerization of PANI into MMT clay galleries. The intercalation was confirmed by measures of X-ray diffraction, and the interlayer distance obtained was changed from 1.47 to 0.36 nm after the polymerization of aniline. Absorption bands of the PANI-ES form were observed at 420 and 800 nm in the UV-vis-NIR

spectrum of the material. In addition, the IR bands at 1568, 1505, 1311 and 1246 cm^{-1} were upshifted in comparison to the free polymer, probably due to intercalation.

Wu et al. [48, 49] also obtained PANI-MMT using ammonium persulphate as an oxidizing agent, the electronic spectrum of the material obtained was very similar to that obtained for secondarily doped PANI-CSA, suggesting that the PANI was obtained in an extended conformation. The formation of PANI-ES was confirmed by the presence of bands at 1489, 1562 and 1311 cm^{-1} in the FTIR spectrum of the material. Despite the high organization level of PANI chains into the MMT clay, the conductivity of the material, ca. $10^{-3} \text{ S.cm}^{-1}$, was not much higher than those obtained previously. The justification of the authors is that there are few polymeric connections between the particles of clay, which significantly reduces the conductivity observed for the material. Later, other authors reported the synthesis of PANI into MMT clay by the intercalation of anilinium ions into MMT followed by oxidation with ammonium persulphate as a standard method to obtain PANI-MMT nanocomposites [50-62].

Some studies were performed by varying the aniline/clay ratio during intercalation, and it was possible to show the increase of interlayer space and the amount of intercalated PANI as well as the increase of the conductivity of the material [63]. The synthesis of PANI with clay in a medium containing surfactants (dodecylbenzenesulfonic acid, DBSA, and camphorsulfonic acid, HCSA) was also used [56-58]. Intercalation was confirmed by X-ray diffraction data, with interlayer distances of $\sim 1.5 \text{ nm}$ and $\sim 1.6 \text{ nm}$ being obtained for composites of PANI-DBSA-MMT and PANI-CSA-MMT, respectively. DC conductivity values for PANI-DBSA-MMT and PANI-CSA-MMT at room temperature were near 0.3 S.cm^{-1} and 1.0 S.cm^{-1} , respectively. The intercalated PANI was also obtained by electrochemical polymerization of aniline, using modified clay electrodes [59], graphite electrode–modified clay [60], Pt electrode–modified clay [61] and electrode stainless steel [62]. Inoue and Yoneyama [59] used a clay-modified electrode and intercalation was performed by immersing the electrode in an aniline solution. An interlayer distance value of 0.54 nm was obtained for MMT clay after immersion. Another work using graphite or Pt electrode modified with clay also reported the formation of PANI, as confirmed by the voltammogram profile curves. The oxidation of a suspension of aniline containing MMT clay intercalated with stainless steel electrodes produced a polymer-MMT–valued interlayer distance of 0.51 nm . The FTIR spectrum of the material presented bands at 1579, 1490 and 1311 cm^{-1} , similar to that obtained by Wu et al. [48] in the chemical polymerization of aniline with ammonium persulphate.

Using resonance Raman (RR) and X-ray absorption spectroscopy, it was possible to show that the structure of intercalated PANI was different from the free PANI structure [64-71]. At early polymerization stages, the presence of radical cations, dications and benzidine dications were observed in the RR spectra by head-to-tail and tail-to-tail coupling of aniline monomers. However, at the final stages, the RR spectra showed different bands, this indicates coupling between the initial segments with the formation of new chromophoric segments. In order to elucidate the structure of the intercalated polymer, the use of XANES spectroscopy was decisive. The XANES spectroscopy opens the possibility of investigating the chemical environments of both clays and polymers.

1.3. X-ray absorption process

A large number of spectroscopic techniques are routinely used in clay and clay materials science research in order to identify elemental, molecular, and crystalline aspects of the samples. Among them, X-ray spectroscopy has a unique capability to obtain atom-specific information as it measures the excitation of core electrons of selected atoms. An X-ray absorption spectrum (XAS) reflects the excitation of a core electron to unoccupied states. As a consequence, it reflects the electronic structure of unoccupied states of a specific atom in the sample; in fact, it is sensitive to the local environment of the selected element. The X-ray intensity (I) is attenuated when it penetrates into a solid material. This decrease is analogous to the Beer–Lambert law [72], i.e., showing that $I_{(x)} = I_0 e^{(-\alpha x)}$ the light intensity decreases due to its penetration into the material (x), since the argument ($-\alpha x$) is a negative function. The decrease is higher when the magnitude of the absorption coefficient (α) is higher. The value of α is a function of the material structure and also the wavelength of the electromagnetic field [73].

X-ray absorption occurs if the incident photon energy is transferred to an electron strongly bounded to the atom. Figure 4 schematically represents the absorption of a K shell electron (1s level) of an atom bonded in a solid material. The absorption coefficient decreases with increasing incident photon energy, but there are sudden changes. These variations correspond to different absorption edges present in the material.

Considering photons with energy lower than the ionization threshold ($h\nu_1$), they are poorly absorbed by the material since there are no unoccupied states below this energy. However, when the energy of the photon reaches the $h\nu_2$ value, there is a sharp increase in the absorption, corresponding to the K edge absorption, this energy is called the ionization threshold for the 1s electron. If the photon energy increases ($h\nu_3$), the atom can be ionized; as a consequence, the absorption coefficient has the same magnitude as the cross-section of the photoelectric effect. If the value of the photon energy continues to increase, absorption begins to degrade, but there may be new sudden jumps, since there are other edges in the absorption material [74-76].

The detection of a chemical element in a material is only the simplest information that is available from the X-ray absorption spectra. In fact, the phenomenon of X-ray absorption is much more complex, and therefore carries much more information. Generally, the absorption spectra are complex; possessing a set of variations that extend over a wide range of energies (tens of units of eV). Figure 5 represents a typical X-ray absorption spectrum, which has a large absorption near the edge and a series of oscillations that will lose intensity as it moves away from the absorption edge. The region near the edge is called XANES (X-ray absorption near-edge structure) and the second one is known as EXAFS (near-edge X-ray absorption fine structure). The XANES region includes a range of energies before the absorption edge up to the beginning of the EXAFS region. The definition of the boundary between these two regions is arbitrary, but there is some consensus that the XANES region extends to 50 eV after the absorption edge. The EXAFS region can be defined as the point where the wavelength of ejected electrons is equal to the distance between the absorber atom and its neighbor atoms, this region can extend up to 1000 eV after the edge [77].

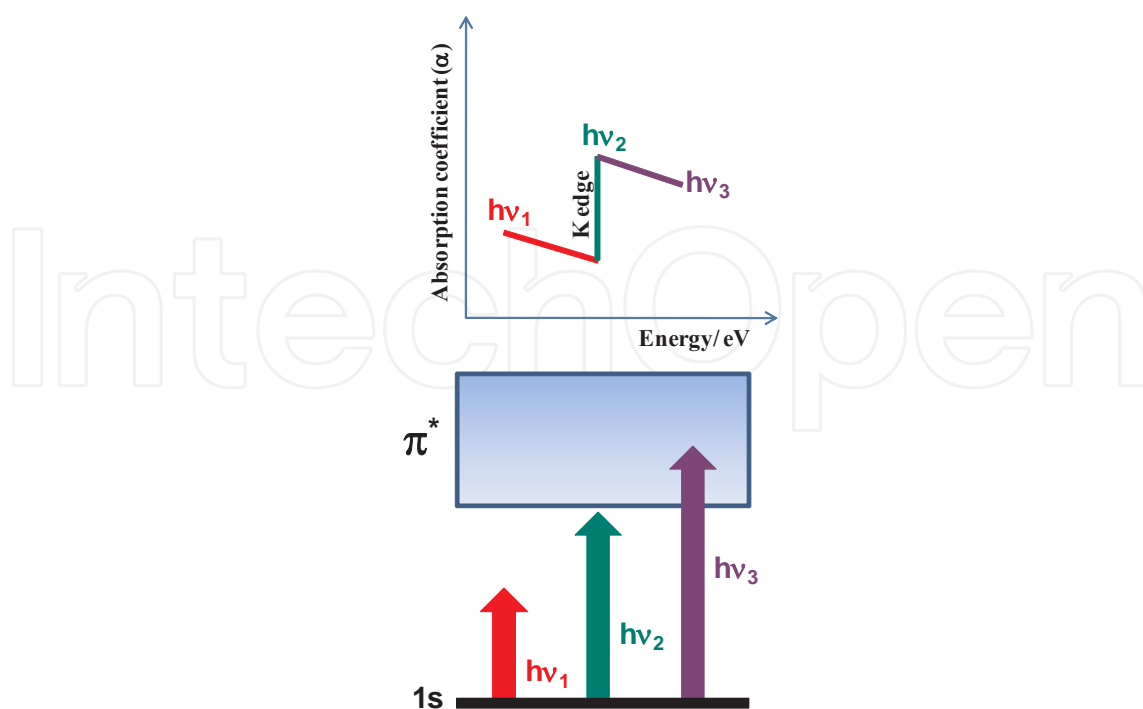


Figure 4. Schematic representation of photons with different energies compared in relation to the ionization threshold for a given material. The $h\nu_1$ photon has low energy to produce ionization; the photon $h\nu_2$ has the exact energy for ionization, so there is a sudden jump in the absorption coefficient that is the experimental characterization of the absorption edge, and finally the photon $h\nu_3$ has much more energy than the edge.

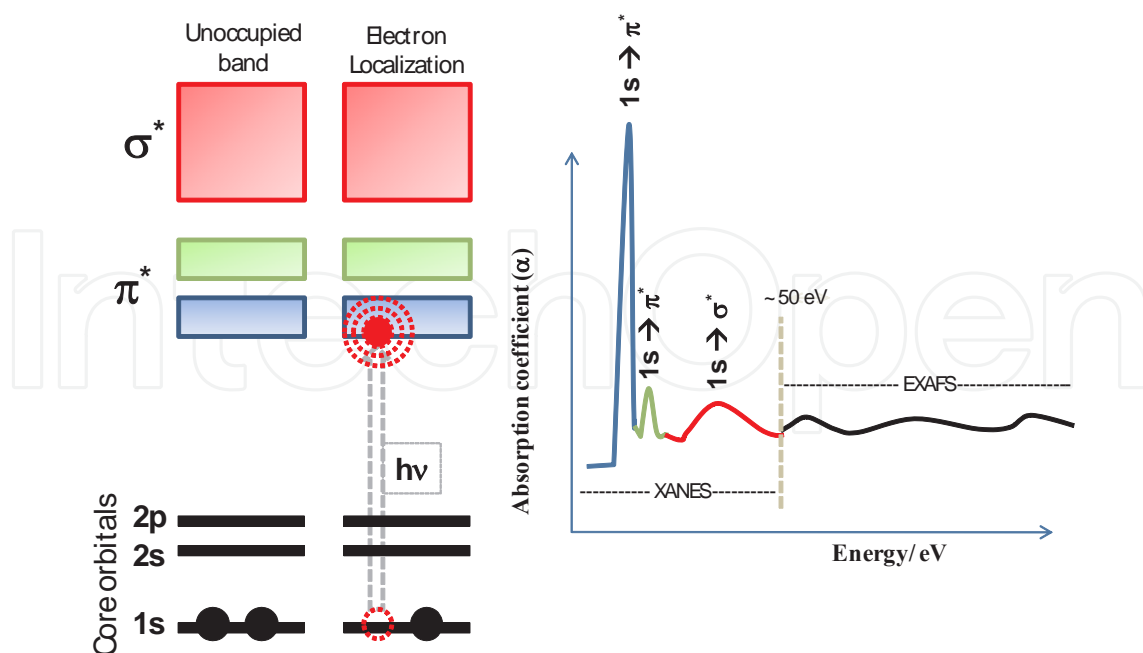


Figure 5. The oscillations in the absorption spectrum were caused by the different final states and contain information related to the structure around the atom that absorbed the radiation.

The EXAFS spectrum originates from interference effects between the excited atoms [77-79]. The wave function of the excited electron propagates beyond the atom and is partially reflected by neighboring atoms. The interference between the wave that spreads and reflected by neighboring atoms causes ripples in the absorption spectrum [78, 79]. The interference can be constructive or destructive, depending on the wavelength associated with the electron and with the interatomic distance. Figure 5 schematically illustrates the origin of the X-ray absorption spectrum. The process can also be visualized as an electronic transition from a core orbital to an unoccupied level with the formation of a core-hole configuration. Photoabsorption coefficient, μ , or photoabsorption cross-section can be generally described by Fermi's "Golden Rule" as

$$\mu \propto \sum_f \left| \langle \psi_f | \exp(i\mathbf{\kappa} \cdot \mathbf{r}) \cdot \mathbf{e} \cdot \mathbf{P} | \psi_i \rangle \right|^2 \times \delta(\hbar\omega - E_f + E_i) \quad (1)$$

where ψ_f and ψ_i are multielectron wave functions at the final and initial states, respectively. The E_f and E_i are the total energy values of the corresponding states. The terms \hbar , ω , $\mathbf{\kappa}$, \mathbf{e} , and \mathbf{r} are energy, wave number vector, the unit vector for the polarization direction of the X-ray and the position of the excited electron, respectively. \mathbf{P} is the sum of the linear momentum operators of electrons. In the XAS, the equation can be approximated using one electron wave functions of the core state ϕ_i , and that of the excited electron, ϕ_f as

$$\mu \propto \sum_f \left(\left| \langle \phi_f | e \cdot \mathbf{r} | \phi_i \rangle \right|^2 + 1/4 \langle \phi_f | (e \cdot \mathbf{r})(\mathbf{\kappa} \cdot \mathbf{r}) | \phi_i \rangle \right) \times \delta(\hbar\omega - E_f + E_i) \quad (2)$$

The core-hole configuration must be included in the one-electron approximation. The electronic relaxation associated with the presence of the core-hole and excited electron need to be accounted for if one wants to reproduce the experimental spectra by first principles calculations using Eq. (2). Under the dipole approximation, where $\mathbf{\kappa}r \ll 1$ and $\exp(i\mathbf{\kappa} \cdot \mathbf{r}) \approx 1$, Eq. (2) can be further simplified to

$$\mu \propto \sum_f \left| \langle \phi_f | e \cdot \mathbf{r} | \phi_i \rangle \right|^2 \times \delta(\hbar\omega - E_f + E_i) \quad (3)$$

There are two different methods to resolve Eq. (2). The first way is called multiple scattering methods, and the second way is by band-structure methods under periodic boundary conditions.

Hence, through treatment with XANES/EXAFS data, it is possible to determine the interatomic distances between the atoms that have suffered excitation and its neighbor atoms [80-82]. The XANES spectrum contains information similar to the EXAFS spectrum, but the information is more difficult to extract from the math standpoint [80, 83, 84]. This is largely due to the different

possibilities of transitions that may occur in the solids in the XANES region, which in the language of scattering theory means that there is multiple scattering in the XANES region. The intensity of absorption is influenced by the number of electrons that occupy the initial state and may therefore participate in absorption, and it also depends on the density of the unoccupied states and the transition momentum. The unoccupied energy levels depend on the oxidation state and the nature of the chemical bond so that this atom, with its neighbors, makes it possible through the XANES spectra, to distinguish the different states of oxidation of this element. The observed modulations into the XANES spectra are also influenced by the oxidation state and nature of chemical bonds of the materials under study. In the following paragraphs, the focus will be on the analysis of XANES spectra at different edges in order to investigate the structure of clays and clay derivate materials. The absorption measurements are only possible in conditions of ultrahigh vacuum (the pressure inside the chamber is ca. 10^{-7} mbar). What is measured is a signal that is directly proportional to the amount of photons absorbed [85]. Upon absorption, emissions occur from the electrons (photoelectrons, electrons Auger and secondary electrons) whose intensities are proportional to the amount of photons absorbed; to keep the sample electrically neutral, it grounds the sample compartment so that the current replacement of the electrons in the sample (typically, the current is of the order of 10^{-12} A) is proportional to the intensity of photons absorbed. It can be described as:

$$I_{(\text{current of replacement of the electrons})} \propto I_{(\text{electrons emitted})} \propto A_{(\text{photons absorbed})}$$

Another concern is about the number of samples that can be placed at one time in the compartment because it takes between 3 and 5 h to reach the required pressure inside the chamber. The arrangement used in our experiments is displayed in Figure 6. Another grooved rod is placed over the main rod to delimit the area (ca. 0.2 cm^2) and prevent the mixing of the samples, since the measurements are made with the rod positioned vertically in the sample chamber.

2. Results and discussion

2.1. XANES data

XANES spectroscopy has been widely used for the investigation of clay structures, metal sites in the clays and also for polymer–clay nanocomposites. By selecting the appropriate energy in the X-ray source, it is possible to investigate the silicon, oxygen and aluminum sites in the clay layers; the metal ions incorporated into the clay layers; as well as the carbon, nitrogen, oxygen and other atoms in the polymer chains. In addition, it is possible to measure the absorption, emission and photoejection signals from the clay materials.

The XANES data supported by DFT calculations were essential to verify the differences into the oxygen sites observed for montmorillonite (MMT) and muscovite mica (MT) clays. The hydroxyl groups localized in these cavities and van der Waals forces contributed significantly to adsorption processes. In both clays, the oxygen surface sites are directly affected by the

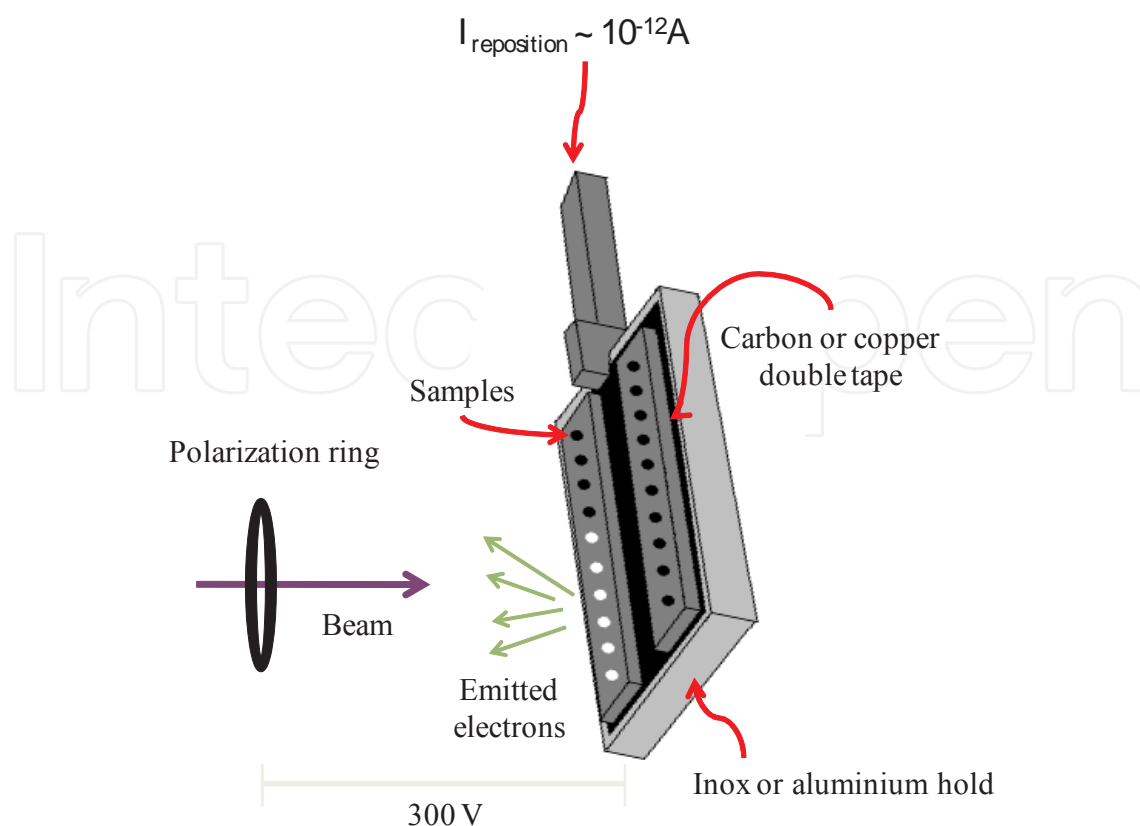


Figure 6. Experimental setup used for XANES measurements.

intralayer interaction through hydroxyl groups. The chemical environment of the hydroxyl groups is distinct in the MMT and MT structures. In fact, the oxygen atoms in the apical position in MT layers are less influenced by van der Waals forces. In addition, the silicon surfaces in MT are more sensitive to the Si-O apical-Al changes and have no disturbance on hydroxyl groups than in MMT clay (86). In another very recent work, the XAS data associated with DFT calculations were used to the study of the electronic structure of synthetic and natural kaolinite clay. This can serve as a model system for engineered and natural clay materials. It was possible to correlate the XANES features with the structural defects present in the clay layers. In both synthetic and natural kaolinite, oxygen replaces hydrogen in the Al (001)-hydroxyl groups on the kaolinite clay sheets. The energy levels associated with these defects are situated in the band gap, and its value decreases by about 3.2 eV as this defect is formed [87].

The presence of metals in clays has also been investigated. Many soils around the globe are contaminated with metals due to inputs from anthropogenic activities; however, the long-term processes that retain these metals in soils remain unclear. Changes in Mn K-edge XANES with soil depth were consistent with a mixing of different pools of Mn. In particular, the proportions of Mn(II)/Mn(III) present in the mineral soil increased relative to Mn(IV) with increasing depth. Mn can be preferentially retained in soils relative to other elements due to this process of uptake and immobilization. The Mn that is taken up into the plant's biomass exists mostly as aqueous and organic Mn(II) compounds that are immobilized as Mn(III)/(IV) oxides during decompo-

sition [88]. Another work studied the interaction of CO₂ and O₂ gases in volcanic soils containing different minerals and clays having Fe(II/III) ions, which was investigated by using the XANES spectroscopy at Fe K-edge. The authors also measured the Fe K-XANES spectra for a great number of reference materials, thus permitting the determination of Fe species during the cycle of CO₂ and O₂ interactions [89].

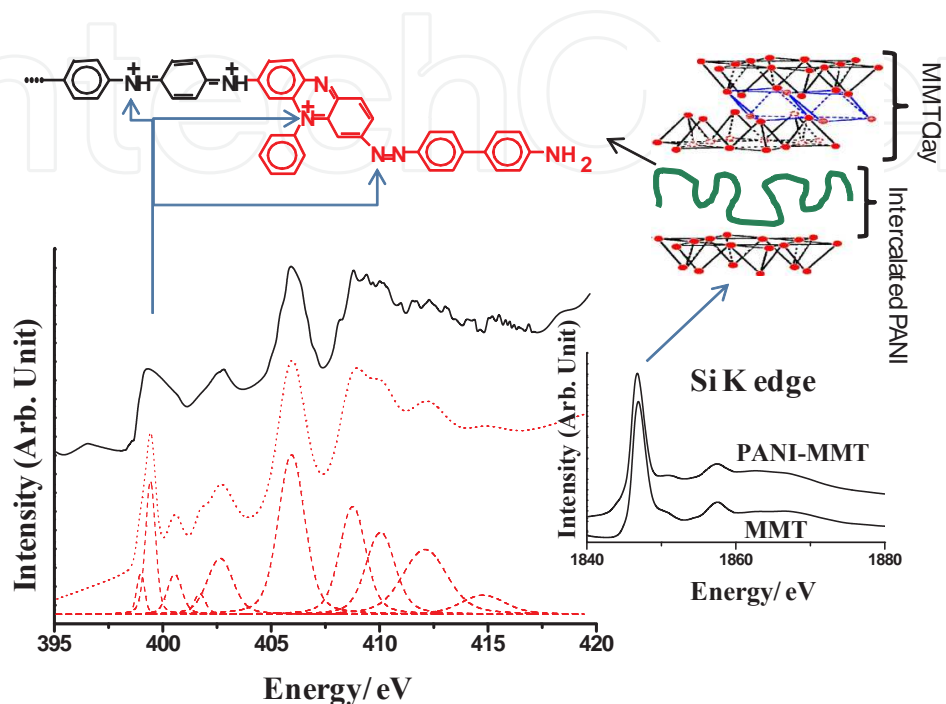


Figure 7. Top: N K XANES spectra of powered samples of PANI-MMT nanocomposites. Experimental spectra are represented by the black continuous line (—). The Voigt bands used in the deconvolution of the experimental spectrum are shown below the experimental data (dashed red line, ---). The sum spectrum of the Voigt bands is also displayed (dotted red line, ...). Deconvolution of the experimental N K XANES spectra was done using SPSS (1995) with Voigt bands (Voigt area mode with varying widths) and linear baseline (linear, D2 mode). The Si K XANES spectra of powered samples of MMT and PANI-MMT are also shown inside the figure. Scheme of PANI-MMT nanocomposites and the intercalated PANI structure are also shown at the top of the figure. Bottom: Tentative assignments of bands observed in N K XANES of PANI-MMT, PBZ-MMT and PpPD-MMT nanocomposites. The band positions were calibrated using the first resonance band value for KNO₃ salt (the beam line has a resolution of 0.1 eV; the N K XANES were calibrated considering the value 405.5 eV, according to ref. [91]).

XANES permits the investigation of the confined polymer into clay galleries, differently from surface techniques, such as X-ray photoelectron spectroscopy. The N K XANES spectrum of polyaniline-montmorillonite prepared by in situ polymerization within the cavities of the MMT clay is displayed in Figure 7. The spectrum of PANI-MMT nanocomposites contains bands with different patterns than the spectra of “free” PANI forms [90]. It is interesting to observe that the structure of MMT clay is not changed because there is no modification of the XANES spectra of MMT at the Si K-edge after PANI formation (see Figure 7). Comparing the set of N K XANES spectra obtained for several organic molecules with nitrogen atoms in different electronic environments [67-69] it was possible to assign the observed bands. Table 1 summarizes the data obtained for PANI-MMT and displays the tentative assignments for the various transitions observed.

Samples				Tentative assignments
PANI-MMT	PBZ-MMT	PpPD-MMT		
bands/cm ⁻¹ (linewidths of the bands/cm ⁻¹)				
398.99 ± 0.05 (0.32)	398.8 ± 0.1 (1.3)	398.8 ± 0.1 (1.5)	1s → π*	—N= of phenazine-like rings and/or — N=N— of azo bonds
399.46 ± 0.05 (0.47)	—	399.64 ± 0.05 (0.88)	1s → π*	—H ₂ N ⁺ = or = N ⁺ = of phenazine-like rings and/or dications of PANI
400.57 ± 0.05 (0.75)	400.18 ± 0.05 (1.4)	400.26 ± 0.05 (0.56)	1s → π*	π-Conjugated nitrogen
401.74 ± 0.05 (0.54)	401.75 ± 0.05 (0.66)	—	1s → π*	Amine nitrogen
402.7 ± 0.1 (1.4)	—	402.2 ± 0.1 (1.1)	1s → π*	Amine nitrogen
406.0 ± 0.1 (1.4)	405.1 ± 0.1 (1.0)	406.0 ± 0.1 (2.0)	1s → π*	—H ₂ N ⁺ — ⁺ NH ₂ —
408.8 ± 0.1 (1.4)	408.7 ± 0.1 (2.4)	—	1s → σ*	—N=N—
410.1 ± 0.1 (1.6)	410.9 ± 0.1 (2.7)	409.2 ± 0.1 (4.8)	1s → σ*	—H ₂ N ⁺ — ⁺ NH ₂ —
412.2 ± 0.1 (2.4)	—	412.7 ± 0.1 (2.7)	1s → σ*	—
414.8 ± 0.1 (2.4)	—	—	1s → σ*	—

Table 1. Data obtained for PANI-MMT and their tentative assignments

It should be mentioned that all N K XANES bands (for 1s → π* and 1s → σ* transitions) observed for intercalated PANI have lower linewidths than those observed for “free” PANI. Structural limitations of the polymer lead to an electronic reorganization and shorter electronic bands; as a consequence, the absorption bands are narrower than those for “free” PANI. The same behavior was observed for polybenzidine (PBZ) and poly(*p*-phenylenediamine) (PpPD) intercalated in the MMT clay. Hence, the N K XANES bands for intercalated PANI can be related to nitrogen atoms bonded in the phenazine-like rings and azo bonds; a similar behavior was also observed for intercalated PpPD. In the case of intercalated PBZ, the bands related to the azo bonds were more intense. The most intense band observed for all spectra of the nanocomposites is near 405–406 eV and can be assigned to protonated azo bonds (hydrazinium bonds); it also confirms the presence of new segments in the intercalated polymers. Finally, it was observed that the structure of confined polymers contains new segments in comparison to that observed for “free” polymers.

2.2. EXAFS data

Much fewer works deal with EXAFS of clays and its derivate materials compared to XANES data. However, it is possible to find studies on the experimental and theoretical determination of Cu(II) sites in clay surfaces and interlayer. Cu(II) in the fully hydrated, Cu-saturated MMT has a singlet 1st derivative XANES spectrum. FEFF calculations show that this singlet feature originates from a quasi-regular octahedral coordination of water molecules around the interlayer Cu(II) atom. All other samples and models have doublet 1st derivative XANES

spectra. FEFF calculations suggest that the doublet features arise from an axially elongated octahedral coordination under the Jahn–Teller effect or square planar coordination. FEFF calculations of the EXAFS spectra as a function of the axial oxygen bond length demonstrate that a destructive interference between backscattering from equatorial oxygen (O-eq) and that from axial oxygen (O-ax) atoms leads to an apparent coordination number (CN) less than six expected for the tetragonal coordination, with the farther, loosely bound axial oxygen atoms making a minor, yet negative, contribution to the CN determined by the EXAFS analysis. This study shows that Cu(II) has interchangeable octahedral, tetragonal and square planar coordination in the MMT interlayer, depending on Cu(II) loading and degree of hydration. The quasi-regular octahedral coordination of the interlayer Cu(II) in MMT is a new finding of this study [92]. In another work [93], the authors studied the sorption mechanism of Cu(II) on hectorite clay. The XAS spectra show an angular dependence between the Cu–O-eq atomic pair and the direction perpendicular to the clay layer plane. Based on the number of Mg/Al and Si nearest neighbors, the Cu(O-eq)₄(O-ax)_{1–2} polyhedron is attached to the clay surface by sharing one to three edges with the structural Al/Mg octahedral and zero to three corners with the Si/Al tetrahedral. Copper has an unusually high coordination on the two dioctahedral aluminous clays, as explained by the presence of distorted empty cavities at their surface, which can accommodate irregular coordination polyhedrals. The steric match between the distorted empty octahedral cavities and the Jahn–Teller distorted Cu polyhedral provides a rationale to explain the higher affinity of Cu(II) for Al octahedral sheets.

3. Perspectives

X-ray absorption spectroscopy is now a powerful tool for the investigation of clays and its derivatives. However, their use in clay science is still in its infancy. In fact, there are plenty of investigation possibilities in clay science, since the studies of surface aspects about the Si, Fe, Al and O sites, where the specificity of the XAS signal can give atomic information around the absorbing atom and up to the characterization of intercalated metals, molecules, biomolecules, and polymers and so on. The XANES data, supported by DFT calculations, were essential to verify the differences in the oxygen sites observed in clays. The hydroxyl groups localized in these cavities and van der Waals forces contribute significantly to adsorption processes. The oxygen surface sites are directly affected by the interlayer interaction through hydroxyl groups. Experimental and theoretical EXAFS studies of clays with Cu(II) show that Cu(II) has interchangeable octahedral, tetragonal and square planar coordination in the clay interlayer, depending on Cu(II) loading and degree of hydration. The angular dependence between the Cu–O-eq atomic pair and the direction perpendicular to the clay layer plane was also observed and the consequences of different coordination sites where the Cu ions can be found. XANES data of intercalated PANI show new bands at 398.8 eV and 405–406 eV. These new bands were assigned to phenazine-like rings and azo bonds in the structure of the polymers (polyaniline, polybenzidine and poly(*p*-phenylenediamine)) within the galleries of Montmorillonite clay. The investigation of the electronic structure of the conducting polymer–clay nanocomposites through XANES spectroscopy has been decisive in the determination of their structure and

also in the study of the interactions between the polymeric chains and the clay layers. The force of these interactions is responsible for guidance in the formation of a polymeric backbone with a distinct structure to that observed in the free polymer. We believe that the XANES/EXAFS studies of the structural pattern of the metal–clay, molecules–clay and polymer–clay nanocomposites will be decisive for their applications.

Acknowledgements

This work is dedicated to my parents (Iara Ap. Morari do Nascimento and Romualdo J. do Nascimento). Many thanks to the National Synchrotron Light Laboratory (LNLS, Campinas-Brazil) for XANES measurements.

Author details

Gustavo M. Do Nascimento*

Address all correspondence to: morari@yahoo.com

Universidade Federal do ABC-CCNH, Campus SBC, Santo André, Brazil

References

- [1] Bergaya, F. & Lagaly, G. (2006). General introduction: Clays, clay minerals, and clay science. In: *Handbook of Clay Science*, Bergaya, F. Theng, B. K. G. & Lagaly, G. (Eds.). 1–18 Elsevier, Amsterdam.
- [2] Hall, P. L. (1987). Clays: their significance, properties, origins and uses. In: *A Handbook of Determinative Methods in Clay Mineralogy*, Wilson, M.J. (Ed.). 1–25, Blackie, Glasgow.
- [3] Guggenheim, S. & Martin, R. T. (1995). Definition of clay and clay mineral: joint report of the AIPEA nomenclature and CMS nomenclature committees. *Clays and Clay Minerals* 43, 255–256 and *Clay Minerals* 30, 257–259.
- [4] Moore, D. M. & Reynolds, R. C. Jr. (1997). *X-ray Diffraction and the Identification and Analysis of Clay Minerals*, 2nd edition. Oxford University Press, Oxford.
- [5] Weaver, C. E. (1989). *Clays, Muds, and Shales*. Elsevier, Amsterdam.
- [6] Brown, G. (1980). Associated minerals. In: *Crystal Structures of Clay Minerals and their X-ray Identification*. Brindley, G.W. & Brown, G. (Eds.). 361–410, Mineralogy Society, London.

- [7] Yariv, S. (2002). Introduction to organo-clay complexes and interactions. In: *Organo-Clay Complexes and Interactions*. Yariv, S. & Cross, H. (Eds.). Marcel Dekker, Inc. New York.
- [8] Wilson, H. (1927). *Ceramics-Clay Technology*. McGraw-Hill Book Co. New York.
- [9] Reis, H. (1927). *Clays, Their Occurrence Properties and Uses*. John Wiley & Sons. Committee on Definition of the Term "Ceramics" (1920). Report of the committee. *Am. Ceramic Soc. Jour.*, 3, 7, 526.
- [10] Norton, F. H. (1952). *Elements of Ceramics*. Cambridge, MA., Addison-Wesley Press.
- [11] Zhang, R., Ni, Q. Q., Natsuki, T. & Iwamoto, M. (2007). Mechanical properties of composites filled with SMA particles and short fibers. *Composite Structures*, Vol. 79, 90–96.
- [12] Meneghetti, P. & Qutubuddin, S. (2006). Synthesis, thermal properties and applications of polymer–clay nanocomposites. *Thermochimica Acta*, Vol. 442, 74–77.
- [13] Hussain, F., Hojjati, M., Okamoto, M. & Gorga, R.E. (2006). Review article: Polymer-matrix nanocomposites, processing, manufacturing, and application: an overview. *Journal of Composite Materials*, Vol. 40, No. 17, 1511–1565.
- [14] Armentano, I., Dottori, M., Fortunati, E., Mattioli, S. & Kenny, J.M. (2010). Biodegradable polymer matrix nanocomposites for tissue engineering: A review. *Polym. Degrad. Stab.*, 95, 11, 2126–2146. 0141-3910.
- [15] Cosoli, P., Scocchi, G., Pricl, S. & Fermaglia, M. (2008). Many-scale molecular simulation for ABS-MMT nanocomposites: Upgrading of industrial scraps. *Micropor. Mesopor. Mat.*, Vol. 107, 169–179.
- [16] Ma, H., Xu, Z., Tong, L., Gu, A. & Fang, Z. (2006). Studies of ABS-graft-maleic anhydride/clay nanocomposites: Morphologies, thermal stability and flammability properties. *Polym. Degrad. Stab.*, Vol. 91, 2951–2959.
- [17] Pandey, J. K., Reddy, K. R., Kumar, A. P. & Singh, R. P. (2005). An overview on the degradability of polymer nanocomposites. *Polym. Degrad. Stab.*, Vol. 88, 234–250.
- [18] Sheng, N., Boyce, M. C., Parks, D.M., Rutledge, G. C., Abes, J. I. & Cohen R.E. (2004). Multiscale micromechanical modeling of polymer/clay nanocomposites and the effective clay particle. *Polymer*, Vol. 45, 487–506.
- [19] LeBaron, P. C., Wang, Z. & Pinnavaia, T. J. (1999). Polymer-layered silicate nanocomposites: an overview. *Appl. Clay Sci.*, Vol. 15, 11–29.
- [20] Thostenson, E. T., Li, C. & Chou, T. W. (2005). Nanocomposites in context. *Compos. Sci. Technol.*, Vol. 65, 491–516.
- [21] Pavlidou, S. & Papaspyrides, C. D. (2008). A review on polymer-layered silicate nanocomposites. *Prog. Polym. Sci.*, Vol. 32, 1119–1198.

- [22] Shirakawa, H. (2001). The discovery of polyacetylene film: the dawning of an era of conducting polymers (Nobel Lecture). *Angew. Chem. Int. Ed.* 40, 14, 2575–2580, 14337851.
- [23] Shirakawa, H. & Ikeda, S. (1971). Infrared spectra of poly(acetylene). *Polym. J.* 2, 2, 231–244, 0032–3896.
- [24] Shirakawa, H. & Ikeda, S. (1974). Cyclotrimerization of acetylene by tris(acetylacetonato)titanium(III)-diethylaluminum chloride system. *J. Polym. Sci. Chem.*, 12, 5, 929–937, 0887–624X.
- [25] MacDiarmid, A. G. (2001). “Synthetic metals”: a novel role for organic polymers (Nobel Lecture). *Angew. Chem. Int. Ed.*, 40, 2581–2590.
- [26] Heeger, A. J. (2001). Semiconducting and metallic polymers: the fourth generation of polymeric materials (Nobel Lecture). *Angew. Chem. Int. Ed.*, 40, 2591–2611.
- [27] Do Nascimento, G. M. & Souza, M. A. (2010). Spectroscopy of nanostructured conducting polymers. In: *Nanostructured Conducting Polymers*. Eftekhari. A.; (Org.). London: Wiley and Sons, 341–375.
- [28] Bissessur, R., DeGroot, D. C., Schindler, J. L., Kannewurf, C. R. & Kanatzidis, M. G. (1993). Inclusion of poly(aniline) into MOO₃. *J. Chem. Soc.: Chem. Commun.*, 8, 687–689. 0022–4936.
- [29] Liu, Y-J., DeGroot, D. C., Schindler, J. L., Kannewurf, C. R. & Kanatzidis, M. G. (1993). Stabilization of anilinium in vanadium(V) oxide xerogel and its post-intercalative polymerization to poly(aniline) in air. *J. Chem. Soc.: Chem. Commun.*, 7, 593–596. 0022–4936.
- [30] Wu, C-G., DeGroot, D. C., Marcy, H. O., Schindler, J. L., Kannewurf, C. R., Liu, Y-J., Hirpo, W. & Kanatzidis, M. G. (1996). Redox intercalative polymerization of aniline in V₂O₅ xerogel. The postintercalative intralamellar polymer growth in polyaniline/metal oxide nanocomposites is facilitated by molecular oxygen. *Chem. Mater.*, 8, 1992–2004. 0897–4756.
- [31] Chang, T., Ho, S. & Chao, K. (1994). Polyaniline intercalated into zeolites, zirconium-phosphate and zirconium arsenate, *J. Phys. Org. Chem.*, 7, 371–376. 0894–3230.
- [32] Kanatzidis, M. G. & Liu, Y. (1993). Topotactic polymerization of aniline in layered uranyl phosphate. *Inorg. Chem.*, 32, 2989–2991. 0020–1669.
- [33] Wu, C-G., DeGroot, D. C., Marcy, H. O., Schindler, J. L., Kannewurf, C. R., Bakas, T., Papaefthymiou, V., Hirpo, W., Yesinowski, J. P., Liu, Y-J. & Kanatzidis, M. G. (1995). Reaction of aniline FEOCL—formation and ordering of conducting polyaniline in a crystalline layered host. *J. Am. Chem. Soc.*, 117, 9229–9242. 0002–7863.

- [34] Moujahid, E. M., Dubois, M., Besse, J-P. & Leroux, F. (2002). Role of atmospheric oxygen for the polymerization of interleaved aniline sulfonic acid in LDH. *Chem. Mater.*, 14, 3799–3807. 0897–4756.
- [35] Wypych, F., Seefeld, N. & Denicoló, I. (1997). Preparation of nanocomposites based on the encapsulation of conducting polymers into 2H-MoS₂ and 1T-TiS₂. *Quimica Nova*, 20, 356–360. 0100–4042.
- [36] Yariv, S. & Michaelian, K. H. (2002). Structure and surface acidity of clay minerals. In *Organo-Clay Complexes and Interactions*. Yariv, S. & Cross, H., (Eds.). Marcel Dekker: New York, 1.
- [37] Hauser, E. A. & Leggett, M. B. (1940). Color reactions between clays and amines. *J. Am. Chem. Soc.*, 62, 1811–1814. 0002–7863.
- [38] Yariv, S., Heller, L. & Safer, Z. (1968). Sorption of aniline by montmorillonite, *Israel J. Chem.*, 6, 741–. 0021–2148.
- [39] Furukawa, T. & Brindley, G. W. (1973). Adsorption and oxidation of benzidine and aniline by montmoillonite and hectorite. *Clays and Clay Miner.*, 21, 279–288. 0009–8604.
- [40] Cloos, P., Moreale, A., Broers, C. & Badat, C. (1979). Adsorption and oxidation of aniline and p-chloroaniline by montmorillonite. *Clay Miner.*, 14, 307–321. 0009–8558.
- [41] Soma, Y. & Soma, M. (1988). Adsorption of benzidines and anilines on Cu-montmorillonites and Fe-montmorillonites studied by resonance Raman-spectroscopy. *Clay Miner.*, 23, 1–15. 0009–8558.
- [42] Soma, Y. & Soma, M. (1989). Chemical-reactions of organic-compounds on clay surfaces. *Environmental Health Perspectives*, 83, 205–214. 0091–6765.
- [43] Soma, Y., Soma, M. & Harada, I. (1983). Raman-spectroscopic evidence of formation of para-dimethoxybenzene cation on Cu-montmorillonite and Ru-montmorillonite. *Chem. Phys. Lett.*, 94, 475–478. 0009–2614.
- [44] Soma, Y., Soma, M. & Harada, I. (1984). The reaction of aromatic-molecules in the interlayer of transition-metal ion-exchanged montmorillonite studied by resonance Raman-spectroscopy. 1. Benzene and para-phenylenes. *J. Phys.Chem.*, 88, 3034–3038. 0022–3654.
- [45] Soma, Y., Soma, M. & Harada, I. (1985). Reactions of aromatic-molecules in the interlayer of transition-metal ion-exchanged montmorillonite studied by resonance Raman-spectroscopy. 2. 4, 4'-Disubstituted biphenyls. *J. Phys. Chem.*, 89, 738–742. 0022–3654.
- [46] Mehrotra, V. & Giannelis, E. P. (1991). Metal-insulator molecular multilayers of electroactive polymers-intercalation of polyaniline in mica-type layered silicates. *Solid State Commun.*, 77, 155–158. 0038–1098.

- [47] Chang, Te-C., Ho, S-Y. & Chao, K-J. (1992). Intercalation of polyaniline in monmorillonite and zeolite, *J. Chin. Chem. Soc.*, 39, 209–212. 0009–4536.
- [48] Wu, Q., Xue, Z., Qi, Z. & Wang, F. (1999). Synthesis and characterization of PAN/CLAY hybrid with extended chain conformation of polyaniline. *Acta Polym. Sin.*, 10, 551–556. 1000–3304.
- [49] Wu, Q., Xue, Z., Qi, Z. & Hung, F. (2000). Synthesis and characterization of PAN/clay nanocomposite with extended chain conformation of polyaniline. *Polymer*, 41, 2029–2032. 0032–3861.
- [50] Biswas, M. & Ray, S. S. (2000) Water-dispersible nanocomposites of polyaniline and montmorillonite, *J. Appl. Polym. Sci.*, 77, 2948–2956. 0021–8995.
- [51] Do Nascimento, G. M. (2013). Synthesis, characterization and applications of conducting polymer–clay nanocomposites. In: *Conducting Polymers: Synthesis, Properties and Applications*. Luiz Carlos Pimentel Almeida. (Org.). 3ed. New York: Nova Science Publishers, Inc., 155–178.
- [52] Lee, D. K., Lee, S. H., Char, K. & Kim, J. (2000). Expansion distribution of basal spacing of the silicate layers in polyaniline/Na⁺-montmorillonite nanocomposites monitored with X-ray diffraction. *Macromol. Rapid Commun.*, 21, 1136–1139. 1022–1336.
- [53] Lee, D., Char, K., Lee, S. W., Park, Y. W. (2003). Structural changes of polyaniline/montmorillonite nanocomposites and their effects on physical properties. *J. Mater. Chem.*, 13, 2942–2947. 0959–9428.
- [54] Yeh, J-M., Liou, S-J., Lai, C-Y., Wu, P-C. & Tsai, T-Y. (2001). Enhancement of corrosion protection effect in polyaniline via the formation of polyaniline-clay nanocomposite materials. *Chem. Mater.*, 13, 1131–1136. 0897–4756.
- [55] Zeng, Q. H., Wang, D. Z., Yu, A. B., Lu, G. Q. (2002). Synthesis of polymer–montmorillonite nanocomposites by in situ intercalative polymerization. *Nanotechnology*, 13, 549–553. 0957–4484.
- [56] Kim, B. H., Jung, J. H., Joo, J., Kim, J. W. & Choi, H. J. (2000). Charge transport and structure of nanocomposites of polyaniline and inorganic clay. *J. Korean Phys. Soc.*, 36, 366–370. 0374–4884.
- [57] Kim, B. H., Jung, J. H., Kim, J. W., Choi, H. J. & Joo, J. (2001). Effect of dopant and clay on nanocomposites of polyaniline (PAN) intercalated into Na⁺-montmorillonite (N⁺-MMT). *Synth. Met.*, 121, 1311–1312. 0379–6779.
- [58] Kim, B. H., Jung, J. H., Kim, J. W., Choi, H. J. & Joo, J. (2001). Physical characterization of polyaniline-Na⁺-montmorillonite nanocomposite intercalated by emulsion polymerization. *Synth. Met.*, 117, 115–118. 0379–6779.
- [59] Inoue, H. & Yoneyama, H. (1987). Electropolymerization of aniline intercalated in montmorillonite. *J. Electroanal. Chem.*, 233, 291–294. 0022–0728.

- [60] Orata, D. & David, S. K. (2000). A comparative study of the electrochemical/electrodegradation of polyaniline from aniline loaded in a clay-mineral/polyaniline composite matrix to that of the bulk solution. *React. Funct. Polym.*, 43, 133–138. 1381–5148.
- [61] Feng, B., Su, Y., Song, J. H. & Kong, K. C. (2001). Electropolymerization of polyaniline/montmorillonite nanocomposite, *J. Mater. Sci. Lett.*, 20, 293–294. 0261–8028.
- [62] Chen, K. H. & Yang, S. M. (2003). Synthesis of polyaniline-modified montmorillonite nanocomposite. *Synth. Met.*, 135, 1–3, 51–52. 0379–6779.
- [63] Jara, P., Justiniani, M., Yutronic, N. & Sobrados, I. (1998). Syntheses and structural aspects of cyclodextrin/dialkylamine inclusion compounds. *J. Incl. Phenom.*, 32, 1–8. 0923–0750.
- [64] Do Nascimento, G. M. & Temperini, M. L. A. (2008). Structure of polyaniline formed in different inorganic porous materials: A spectroscopic study. *Eur. Polym. J.*, 44, 3501–3511.
- [65] Do Nascimento, G. M. & Temperini, M. L. A. (2011). Spectroscopic study of the polymerization of intercalated anilinium ions in different montmorillonite clays. *J. Mol. Struct.*, 1002, 63–69.
- [66] Do Nascimento, G. M., Constantino, V. R. L. & Temperini, M. L. A. (2002). Spectroscopic characterization of a new type of conducting polymer–clay nanocomposite. *Macromolecules*, 35, 7535–7537.
- [67] Do Nascimento, G. M., Landers, R., Constantino, V. R. L. & Temperini, M. L. A. (2004). Aniline polymerization into montmorillonite clay: a spectroscopic investigation of the intercalated conducting polymer. *Macromolecules*, 37, 9373–9385.
- [68] Do Nascimento, G. M., Constantino, V. R. L. & Temperini, M. L. A. (2004) Spectroscopic characterization of doped poly(benzidine) and its nanocomposite with cationic clay. *J. Phys. Chem. B*, 108, 5564–5571.
- [69] Do Nascimento, G. M., Landers, R., Constantino, V. R. L. & Temperini, M. L. A. (2006). Spectroscopic characterization of polyaniline formed in the presence of montmorillonite clay. *Polymer*, 47, 6131–6139.
- [70] Do Nascimento, G. M., Barbosa, P. S. M., Constantino, V. R. L. & Temperini, M. L. A. (2006). Benzidine oxidation on cationic clay surfaces in aqueous suspension monitored by in situ resonance Raman spectroscopy. *Colloids Surf. A: Physicochem. Eng. Aspects*, 289, 39–46.
- [71] Do Nascimento, G. M., Padilha, A. C. M., Constantino, V. R. L. & Temperini, M. L. A. (2008). Oxidation of anilinium ions intercalated in montmorillonite clay by electrochemical route. *Colloids Surf. A: Physicochem. Eng. Aspects*, 318, 245–253.
- [72] Atkins, P. W. (1994). *Physical Chemistry*; Oxford University Press: Oxford-London, page 545.

- [73] Margaritondo, G. (2002). *Elements of Synchrotron Light for Biology, Chemistry and Medical Research*. Oxford University Press: New York, Chapter 3.
- [74] Margaritondo, G. (1988). *Introduction to Synchrotron Radiation*. Oxford University Press: New York, Chapter 2.
- [75] Durham, P. J. (1988). In *Chemical Analysis*; Koningsberger, D. C., Prins, R., Eds.; John Wiley & Sons: USA, 92, Chapter 2, page 53.
- [76] Thompson, A. C. & Vaughan, D. (2001). *X-ray Data Booklet Compiled and Edited by Lawrence Berkeley National Laboratory*; Lawrence Berkeley National Laboratory University of California Berkeley: California.
- [77] Bianconi, A. (1980). Surface x-ray absorption-spectroscopy—surface EXAFS and surface XANES. *Appl. Surf. Sci.*, 6, 392–418. 0169–4332.
- [78] Lee, P. A., Citrin, P. H., Eisenberger, P. & Kincaid, B. M. (1981). Extended x-ray absorption fine-structure—its strengths and limitations as a structural tool. *Rev. Mod. Phys.* 53, 769–806. 0034–6861.
- [79] Stern, E. A. (1988). In *Chemical Analysis*. Koningsberger, D. C. & Prins, R., Eds., John Wiley & Sons: USA, 92, Chapters 1 and 3.
- [80] Abruña, H. D. (1989). In *Modern Aspects of Electrochemistry*; Bockris, J. O'M., White, R. E. & Conway, B. E., Eds.; Plenum Press: New York, 20, Chapter 4, page 265.
- [81] Parsons, J. G., Aldrich, M. V. & Gardea-Torresdey, J. L. (2002). Environmental and biological applications of extended X-ray absorption fine structure (EXAFS) and X-ray absorption near edge structure (XANES) spectroscopies. *Appl. Spect. Rev.*, 37, 187–222. 0570–4928.
- [82] Bianconi, A. (1988). In *Chemical Analysis*; Koningsberger, D. C. & Prins, R., Eds.; John Wiley & Sons: USA, 92, Chapter 11, page 573.
- [83] Manne, R. & Åberg, T. (1970). Koopmans' theorem for inner-shell ionization. *Chem. Phys. Lett.*, 7, 282–284. 0009–2614.
- [84] Manne, R. & Åberg, T. (1978). In *Benchmark Papers in Physical Chemistry and Chemical Physics/2:X-ray Photoelectron Spectroscopy*. Carlson, T. A., Ed.; Dowden, Hutchinson & Ross, Inc.: Stroudsburg-Pennsylvania, Chapter 3, page 124.
- [85] Heald, S. M. (1988). In *Chemical Analysis*; Koningsberger, D. C. & Prins, R., Eds.; John Wiley & Sons: USA, 92, Chapter 3, page 87.
- [86] Alvim, R. S. & Miranda, C. R. (2015). First principles characterization of silicate sites in clay surfaces. *Phys. Chem. Chem. Phys.*, 17, 4952–4960. 1463–9076.
- [87] Pietzsch, A., Nisar, J., Jämstorp, E., Gråsjö, J., Arhammar, C., Ahuja, R., J-E. Rubensson, J. E. (2015). Kaolinite: Defect defined material properties – A soft X-ray and first principles study of the band gap. *J. Electron Spectrosc.*, 202, 11–15. 0368–2048.

- [88] Herndon, E. M., Martínez C. E. & Brantley, S. L. (2014). Spectroscopic (XANES/XRF) characterization of contaminant manganese cycling in a temperate watershed. *Biogeochemistry*, 121, 505–551. 0168–2563.
- [89] Rennert, T., Eusterhues, K., De Andrade, V., Totsche, K. U. (2012). Iron species in soils on a mofette site studied by Fe K-edge X-ray absorption near-edge spectroscopy. *Chem. Geology.*, 332–333, 116–123. 0009–2541.
- [90] Do Nascimento, G. M. (2013). X-ray absorption spectroscopy of nanostructured polyanilines. *Chemical Papers*, 67, 8, 933–945. 0366–6352.
- [91] Vinogradov, A. S. & Akimov, V. N. (1998). X-ray absorption study of the spectrum of free electronic states in a KNO₃ crystal. *Opt. Spectrosc.*, 85, 53–59. 0030–400X.
- [92] Hyun, S. P. & Hayes, K. F. (2015). X-ray absorption spectroscopy study of Cu(II) coordination in the interlayer of montmorillonite. *Appl. Clay Sci.*, 107, 122–130. 0169–1317.
- [93] Schlegel, M. L. & Manceau, A. (2013). Binding mechanism of Cu(II) at the clay-water interface by powder and polarized EXAFS spectroscopy. *Geochim. Cosmochim. Acta*, 113, 113–124. 0016–7037.

